THE JOURNAL OF BIOLOGICAL CHEMISTRY VOL. 285, NO. 19, pp. 14806–14814, May 7, 2010
Printed in the U.S.A.

Ternary Complex of Transforming Growth Factor-β1 Reveals Isoform-specific Ligand Recognition and Receptor Recruitment in the Superfamily*[S]

Received for publication, October 28, 2009, and in revised form, January 4, 2010 Published, JBC Papers in Press, March 5, 2010, DOI 10.1074/jbc.M109.079921

Sergei Radaev[‡], Zhongcheng Zou[‡], Tao Huang[§], Eileen M. Lafer[§], Andrew P. Hinck[§], and Peter D. Sun[‡1]

From the [‡]Structural Immunology Section, Laboratory of Immunogenetics, NIAID, National Institutes of Health, Rockville, Maryland 20852 and the [§]Department of Biochemistry, University of Texas Health Science Center, San Antonio, Texas 78229

Transforming growth factor (TGF)-β1, -β2, and -β3 are 25-kDa homodimeric polypeptides that play crucial nonoverlapping roles in embryogenesis, tissue development, carcinogenesis, and immune regulation. Here we report the 3.0-Å resolution crystal structure of the ternary complex between human TGF-β1 and the extracellular domains of its type I and type II receptors, TβRI and TβRII. The TGF-β1 ternary complex structure is similar to previously reported TGF-β3 complex except with a 10° rotation in TβRI docking orientation. Quantitative binding studies showed distinct kinetics between the receptors and the isoforms of TGF-β. TβRI showed significant binding to TGF-β2 and TGF-β3 but not TGF-β1, and the binding to all three isoforms of TGF-β was enhanced considerably in the presence of TβRII. The preference of TGF-β2 to TβRI suggests a variation in its receptor recruitment *in vivo*. Although TGF-β1 and TGF-β3 bind and assemble their ternary complexes in a similar manner, their structural differences together with differences in the affinities and kinetics of their receptor binding may underlie their unique biological activities. Structural comparisons revealed that the receptor-ligand pairing in the TGF-β superfamily is dictated by unique insertions, deletions, and disulfide bonds rather than amino acid conservation at the interface. The binding mode of TβRII on TGF-β is unique to TGF-βs, whereas that of type II receptor for bone morphogenetic protein on bone morphogenetic protein appears common to all other cytokines in the superfamily. Further, extensive hydrogen bonds and salt bridges are present at the high affinity cytokine-receptor interfaces, whereas hydrophobic interactions dominate the low affinity receptor-ligand interfaces.

Transforming growth factor (TGF)-β[2] isoforms regulate the growth and differentiation of many cell types involved in normal development, immune function, and carcinogenesis (1–3). TGF-βs are the founding members of a highly diversified family of signaling ligands and receptors, known as the TGF-β superfamily. To date the superfamily consists of more than 30 growth factors and cytokines, including TGF-βs, bone morphogenetic proteins (BMPs), activins, inhibins, nodal, Müllerian inhibiting substance, growth differentiation factors, and others (4). TGF-βs and related factors signal through two single-pass transmembrane receptors, known as the type I and type II receptors. These two receptor types have the same overall domain structure, including an extracellular ligand-binding domain displaying a three-finger toxin fold, a single transmembrane helix, and a cytosolic serine-threonine kinase domain. Signaling is initiated by the ligand, which binds the receptor extracellular domains, bringing them together and triggering a phosphorylation cascade, whereby the type II phosphorylates the type I, and the type I phosphorylates Smads, the cytoplasmic effectors of the pathway (3).

Specificities have been determined based on cell-based affinity labeling studies with radiolabeled ligands and have enabled the identification of major ligands for most receptors of the superfamily, including those specific for BMPs, TGF-βs, activins, and Müllerian inhibiting substance (4). Structural studies of the BMP and TGF-β receptor extracellular domains complexed to their cognate ligands have revealed that although ligands and receptors of the different subfamilies share the same overall fold, they nevertheless bind and assemble their receptors in ways that are entirely distinct (5–9). The distinct mode of ternary complex assembly for BMP-2 and TGF-β underscores the complexity governing the ternary complex assembly. That also raises the question about which mode of type II receptor binding is realized for other cytokines in the superfamily and what are the critical factors determining receptor specificity and promiscuity. In addition, the cytokines outnumber their receptors in the family with at least 29 ligands in mammals signaling through seven type I and six receptors (3, 10–12), raising the question of combinatorial ligand recognition in the superfamily. Further, little is known regarding the underlying mechanisms by which ligands of particular subfamilies induce their specific activities. Although the three TGF-β isoforms, TGF-β1, -β2, and -β3, signal through the same receptors and share significant sequence (71–79% identity) and structural similarity (backbone root mean square deviations (r.m.s.d.) < 1.5 Å) (13–16), they nevertheless carry out unique functions *in vivo* as shown by the severe yet distinct phenotypes

* This work was supported, in whole or in part, by National Institutes of Health Grant GM58670 (to A. P. H.). This work was also supported by NIAID intramural research funding and by Robert A. Welch Foundation Grant AQ1431 (to A. P. H.).

[S] The on-line version of this article (available at http://www.jbc.org) contains supplemental Table S1 and Figs. S1 and S2.

The atomic coordinates and structure factors (code 3KFD) have been deposited in the Protein Data Bank, Research Collaboratory for Structural Bioinformatics, Rutgers University, New Brunswick, NJ (http://www.rcsb.org/).

[1] To whom correspondence should be addressed: 12441 Parklawn Dr., Rockville, MD 20852. Tel.: 301-496-3230; Fax: 301-402-0284; E-mail: psun@nih.gov.

[2] The abbreviations used are: TGF, transforming growth factor; r.m.s.d., root mean square deviation; NCS, noncrystallographic symmetry; BMP, bone morphogenetic protein; BMPRII, type II receptor for BMP; MES, 4-morpholineethanesulfonic acid; RU, response units.

of the isoform-specific TGF-β null mice (17–20). These differences have been attributed to distinct patterns of expression (17–19, 21), yet some evidence suggests that it might also be due to differences in the ligands themselves. For example, the addition of purified exogenous TGF-βs has been shown to lead to different outcomes in a bilateral palatal shelf closing assay, with TGF-β3 promoting complete fusion and TGF-β1 and -β2 promoting only partial fusion (22). The application of purified TGF-β1 and -β3 has been further shown to lead to dramatic differences in cutaneous wound healing, with TGF-β3 preventing and TGF-β1 promoting scarring (23). The objective of this study was to investigate the mechanism by which TGF-βs bind and assemble TβRI and TβRII into a signaling complex, to define the structural principles that underlie TGF-β isoform-specific function through comparison with the TGF-β3 ternary complex, and to define the structural principles governing the combinatorial ligand recognition among TGF-β superfamily receptors.

EXPERIMENTAL PROCEDURES

Protein Expression and Purification—Recombinant human TGF-β1 (residues 279–390 of the mature sequence) was expressed in Chinese hamster ovary lec3.2.8.1 cells as described previously (40). For surface plasmon resonance experiments recombinant human TGF-β2 and TGF-β3 were expressed in *Escherichia coli* and refolded (41). The extracellular domains of human TβRI (residues 7–91) and TβRII (residues 15–130) were expressed in *E. coli*, refolded, and purified as previously reported (31, 42).

Crystallization and Structure Determination—TGF-β1 was first mixed with TβRII and then with TβRI at a molar ratio of ~1:4:4. The ternary complex was separated from the excess of TβRI and TβRII by size exclusion chromatography in 50 mM NaCl, 20 mM Tris-HCl, pH 8.0. Crystals of the TGF-β1·TβRI·TβRII ternary complex were obtained by vapor diffusion in hanging drops at room temperature in 8–15% polyethylene glycol 4000–8000 at pH 6.0–8.0. The complex crystals diffracted to 3.0 Å resolution, belonged to a triclinic space group P1 with cell dimensions $a = 37.70$ Å, $b = 99.35$ Å, $c = 102.7$ Å, $\alpha = 64.01°$, $\beta = 84.47°$, and $\gamma = 84.34°$. The x-ray data sets were collected at the Southeast Regional Collaborative Access Team 22-ID Beamline at the Advanced Photon Source, Argonne National Laboratory. Supporting institutions are listed at the Southeast Regional Collaborative Access Team website. The data were processed and scaled with HKL2000 (43).

The structure was solved by the molecular replacement method using the structures of TGF-β2 (Protein Data Bank code 2TGI), the extracellular domains of TβRII (Protein Data Bank code 1M9Z), and BMPR-Ia (Protein Data Bank code 1REW) as search models. The solutions for TGF-β1 and TβRII were obtained with the program Phaser, and the solution for TβRI was obtained using Evolutionary programming for molecular replacement (44, 45). There are two ternary complexes in each asymmetric unit that were modeled using the programs O and COOT (46, 47). The structure was refined using a maximum likelihood target function of CNS v1.1 (48) with a 2-fold noncrystallographic (NCS) constraint between the two ternary complexes. Final rounds of the refinement were carried out with phenix.refine (49) without NCS constraints. Several programs from CCP4 program suite were used throughout model building and refinement (50).

Surface Plasmon Resonance—Binding studies were performed with a BIAcore 3000 instrument (GE Healthcare) and were analyzed using the software package Scrubber2 (Biologic Software). TGF-βs were biotinylated and captured on carboxymethyl dextran (CM5) chips to which 5000 response units (RU) streptavidin had been covalently attached to all four flow cells using an amine coupling kit (GE Healthcare). TGF-β2 was biotinylated in 25 mM MES, pH 4.8, by first activating it with a 10-fold molar excess of 1-ethyl-3-(3-dimethylaminopropyl) carbodiimide hydrochloride (GE Healthcare) in the presence of a 25-fold molar excess of *N*-hydroxysuccinimide (GE Healthcare) and then by adding a 100-fold molar excess of amine-PEO_3-biotin (Pierce). TGF-β1 and -β3 were biotinylated by first complexing the protein with an excess of TβRII (4 equivalents) or TβRI and TβRII (4 equivalents each) followed by the addition of a 10-fold molar excess of sulfo-*N*-hydroxysuccinimide-LC-LC-Biotin (Pierce). Singly biotinylated TGF-β1 and -β3 were separated from doubly and multiply biotinylated forms by applying them to a Source S cation exchange column (GE Healthcare) in the presence of 30% isopropanol at pH 4.0. To ensure the reliability of the results, surface densities of captured TGF-βs were kept at 50–300 RU. TβRII binding data for TGF-β1 and -β3 were collected using ligands that had been modified in the presence of TβRII, whereas TβRI binding data (both alone and in the presence of 4 μM TβRII) were collected using ligands that had been modified in the presence of both TβRI and TβRII.

Binding assays were performed by injecting 2-fold serial dilutions of the receptor in duplicate or triplicate in HBS-EP buffer (GE Healthcare) at a flow rate of either 5 μl/min (equilibrium experiments for interactions with slow association times) or 50–100 μl/min (equilibrium experiments for interactions with fast association times and kinetic experiments). The surfaces were regenerated by a brief injection of 10 mM glycine, pH 2.5 (30-s contact time at a flow rate of 50–100 μl/min). Instrument noise was removed by referencing the data against at least three blank buffer injections. A very small background signal, caused by the nonspecific absorption of the receptors to the surfaces, was removed by referencing the data against a flow cell containing only immobilized streptavidin. Equilibrium analyses were performed on steady state measurements using the equilibrium binding response near the end of the injection. Kinetic analyses were performed by global fitting with a simple 1:1 model. Standard errors were obtained from the variation among the derived parameters from independent measurements using Origin Software.

RESULTS AND DISCUSSION

Structure of TGF-β1·TβRI·TβRII Ternary Complex—The structure of a human TGF-β1·TβRI·TβRII ternary complex was determined to 3.0-Å resolution (Table 1). One TGF-β1 homodimer binds to two TβRI and two TβRII receptors forming a 2:2:2 complex (Fig. 1). Each asymmetric unit contains two complexes related by a NCS 2-fold symmetry. Electron densi-

TABLE 1
Data collection and refinement statistics

Data collection	
Space group	*P*1
Unit cell (Å)	$a = 37.70$, $b = 99.35$, $c = 102.7$, $\alpha = 64.01°$, $\beta = 84.47°$, $\gamma = 84.34°$
Resolution limit (Å)	3.0
Unique reflections	23,426 (1223)[d]
Redundancy	1.9 (1.6)
Completeness (%)	87.9 (44.9)
R_{sym} (%)[a]	8.0 (24.5)
$<I/\sigma I>$	9.2 (2.0)
Refinement	
Resolution (Å)	46.0-3.0
No. reflections	22,145
No. protein atoms[b]	9062
No. solvent atoms	93
R_{cryst} (%)	21.7 (30.0)
R_{free} (%)[c]	26.8 (38.8)
r.m.s.d. bond lengths (Å)	0.003
r.m.s.d. bond angles (°)	0.63

[a] $R_{sym} = 100 \times \Sigma|I_h - <I_h>|/SI_h$, where $<I_h>$ is the mean intensity of multiple measurements of symmetry equivalent reflections.
[b] Total number of atoms in one asymmetric unit, which contains two complexes. The second complex was generated by NCS operator. Refinement was carried out using strict NCS constraints.
[c] R_{free} was calculated using a test set of 5%.
[d] The values in parentheses are for highest resolution shell 3.11-3.00 Å.

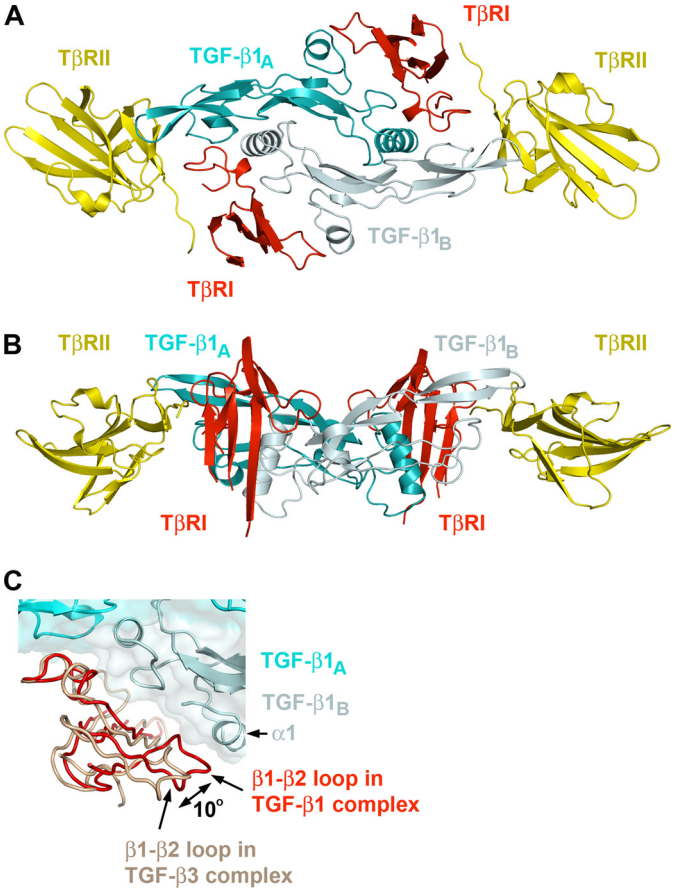

FIGURE 1. **Ribbon drawing of the TGF-β1 ternary complex.** *A*, top view of the complex. *B*, side view rotated ~90° compared with *A*. TGF-β1 monomers TGF-$\beta1_A$ and TGF-$\beta1_B$ are colored *cyan* and *pale cyan*, respectively. TβRI and TβRII are colored *red* and *yellow*, respectively. *C*, relative positions of type I receptors from TGF-β1 (*red*) and TGF-β3 (*salmon*) ternary complexes. This figure and all subsequent ribbon drawings are prepared using the PyMOL molecular graphics system.

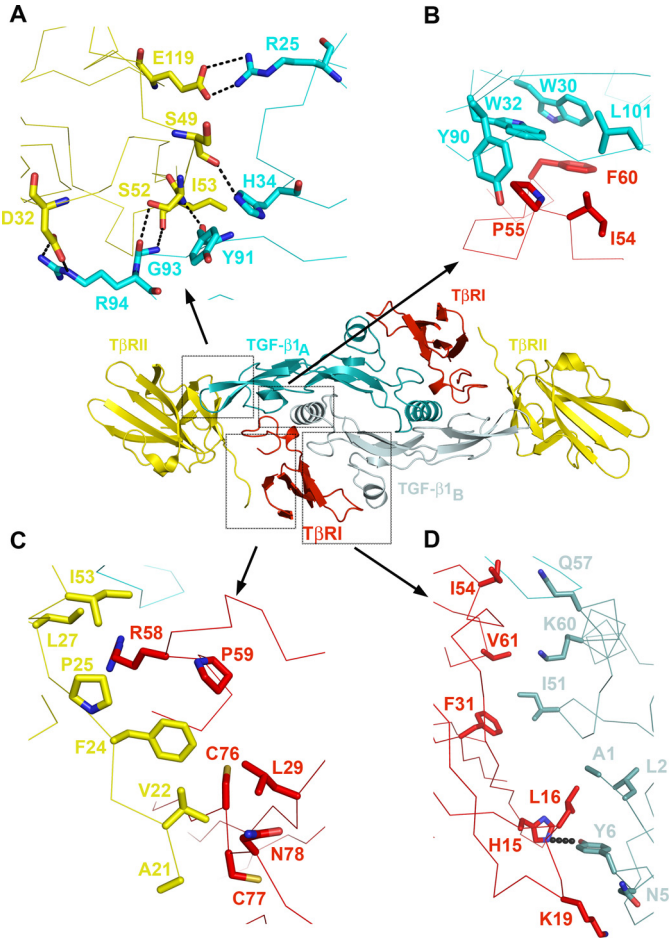

FIGURE 2. **Detailed views of the receptor/ligand interfaces in TGF-β1 ternary complex.** *A*, TβRII/TGF-β1 hydrogen bonding network. *B*, TβRI/TGF-$\beta1_A$ interface. *C*, TβRI/TβRII interface. *D*, TβRI/TGF-$\beta1_B$ interface. The *central inset* is placed as a reference to show location of different interfaces. All of the detailed interfaces are shown as Cα traces. Major residues involved in the interactions are shown in *stick* representation, colored according to the molecule and labeled. Hydrogen bonds are shown as *dotted lines*.

ties for all 112 residues in both chains of TGF-β1 homodimer, for residues 20–126 of TβRII, and for residues 9–85 of TβRI were well defined except for two loop regions of TβRI between residues 36 and 38 and between residues 64 and 71 that correspond to the tips of finger 2 and finger 3 of the three-finger toxin fold. All interface residues between the three components of the complex were well resolved. The overall assembly of the ternary complex is very similar to the reported structure of TGF-β3·TβRI·TβRII complex (Protein Data Bank code 2PJY) with an r.m.s.d. of 1.14 Å for 357 Cα atoms (supplemental Fig. S1) (7). In the center of the complex, butterfly-like shaped TGF-β1 homodimer (TGF-$\beta1_A$ and TGF-$\beta1_B$ subunits) interacts with two TβRII and two TβRI receptors (Fig. 1). The structure of the TGF-β monomer was originally described as a slightly curved left hand with α1 and α3 helixes forming the thumb and the heel of the hand and two antiparallel β-sheets forming its four fingers (13). Both receptors TβRI and TβRII demonstrate three-finger toxin fold with some differences in the shape, length, and secondary structure of their first and third fingers. The ternary complex defines three pairwise interaction interfaces between TGF-β1 and TβRI, TGF-β1 and

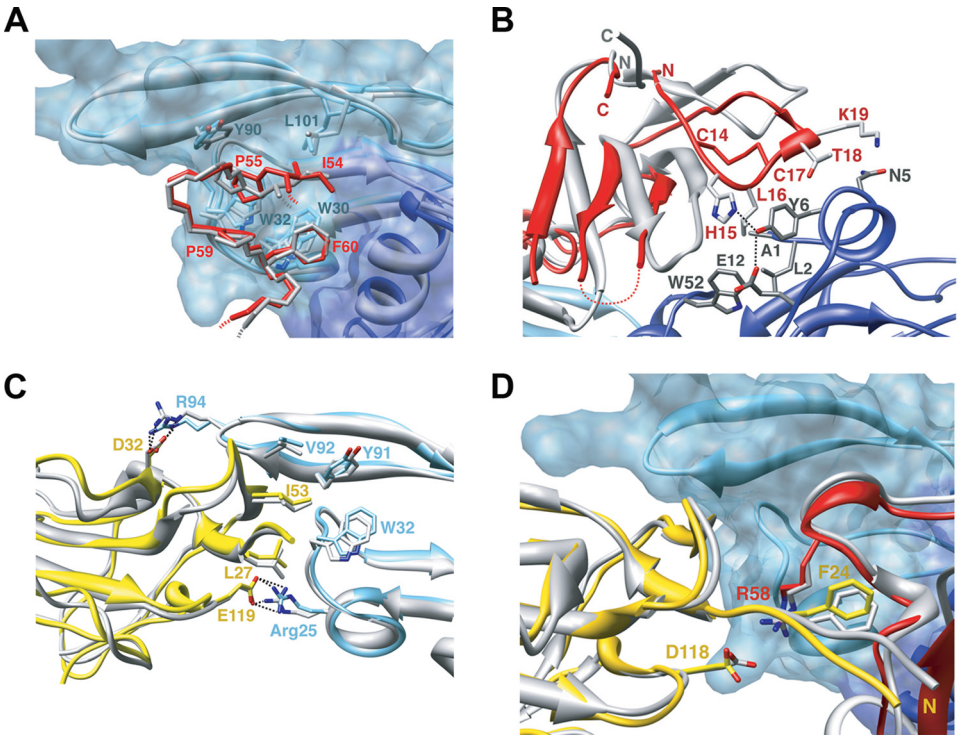

FIGURE 3. **Structural superposition between TGF-β1 and TGF-β3 ternary complexes.** *A* and *B*, interface contacts between TβRI and TGF-$\beta1_A$ (*A*) and between TβRI and the helix α1 of TGF-$\beta1_B$ (*B*). TGF-β1 complex is colored in *light* and *dark blue* for TGF-$\beta1_A$ and TGF-$\beta1_B$ monomers and *red* for TβRI, whereas TGF-β3 complex is in *gray*. *C* and *D*, the TβRII/TGF-β interface (*C*) and the TβRI/TβRII interface region (*D*) with TGF-β1 complex colored in *light blue* for TGF-β1, *red* for TβRI, and *yellow* for TβRII, whereas the TGF-β3 complex is in *gray*.

TβRII, and between TβRI and TβRII, burying 1518-, 940-, and 740-Å^2 solvent-accessible areas, respectively. There are no significant conformational changes in TGF-β and TβRII upon complex formation. Superposition of the current receptor with the unbound TβRII (Protein Data Bank code 1M9Z) resulted in an r.m.s.d. of 0.5 Å for 100 Cα atoms. Similarly, the receptor-bound TGF-β1 can be superimposed with unbound TGF-β1 (minimized average NMR structure, Protein Data Bank code 1KLC), TGF-β2 (Protein Data Bank code 2TGI), and TGF-β3 (Protein Data Bank codes 1TGK and 1TGJ), resulting in an r.m.s.d. of 0.9–1.5 Å for 100–109 Cα atoms.

Recognition of TGF-β1 by the Type I Receptor—The type I receptor contacts both monomers of TGF-β1, generating two primarily hydrophobic patches of the interface burying 370 and 1150 Å^2 of accessible-solvent area with TGF-$\beta1_A$ and TGF-$\beta1_B$, respectively (Fig. 2 and supplemental Table S1). The interface between TGF-$\beta1_A$ and TβRI consists of Trp^{30}, Trp^{32}, Tyr^{90}, and Leu^{101} of the "palm" side of TGF-$\beta1_A$ fingers and Ile^{54}, Pro^{55}, and Phe^{60} from TβRI. This interface is well conserved in the structure of TGF-β3 ternary complex as well as among the sequences of three TGF-β isoforms (Figs. 3*A* and 4*A*). The second patch consists of Ala^1, Leu^2, Asn^5, and Tyr^6 from α1-helix and Ile^{51}, Gln^{57}, and Lys^{60} from α3-helix of TGF-$\beta1_B$ contacting His^{15}, Leu^{16}, Lys^{19}, Phe^{31}, Ile^{54}, and Val^{61} from TβRI with one hydrogen bond between the side chain of Tyr^6 of TGF-β1 and His^{15} of TβRI. Interestingly, in the TGF-β3 ternary complex structure, TβRI is rotated ~10° away from TGF-β as calculated by program HINGE (Fig. 1*C* and supplemental Fig. S1*B*) (24), resulting in a partial solvent exposure and a 400-Å^2 reduction of buried solvent-accessible area at this interface between TβRI and TGF-$\beta3_B$. There is, however, one hydrophobic interaction between Thr^{67} of TGF-$\beta3_B$ and Val^{71} of TβRI, which is absent in current TGF-β1 complex because of a partial disorder of β4-β5 loop around Val^{71} of TβRI.

TβRI and BMPR-Ia dock to their ligands at a closely related site (Site I) with a 10–30° difference in their receptor orientations (Fig. 5*A*). However, both the identity and position of interface residues vary considerably between the type I receptors (Fig. 4), suggesting a promiscuous recognition at Site I. Nevertheless, no cross-reactivity was observed between BMPR-Ia and TβRI (1, 25). Previously (7), a prehelix loop region (between the β4-β5 strands) was suggested to be partially responsible for TβRI specificity. The current structure points to the new area of interactions between the N-terminal loop of TβRI (β1-β2 loop) and the α1-helix of TGF-β1. The corresponding loop in BMPR-Ia contains insertions that potentially would hinder BMPR-Ia binding to the α1-helix of TGF-β (Fig. 5*A*). This α1-helix is stabilized by a Cys^7–Cys^{16} disulfide bond in TGF-βs but is either absent or disordered in the structures of all BMPs, activin, and growth differentiation factor 5 (5–6, 26–29). Interestingly, ALK1 and ALK2 also have a short β1-β2 loop that correlates with their permissive recognition of both TGF-βs and BMPs.

Recognition of TGF-β1 by the Type II Receptor—The interactions between TGF-β1 and TβRII involve five TGF-β1 residues (Arg^{25}, His^{34}, Tyr^{91}, Gly^{93}, and Arg^{94}) at the tips of its fingers and seven TβRII residues (Phe^{30}, Asp^{32}, Ser^{49}, Ile^{50}, Ser^{52}, Ile^{53}, and Glu^{119}) on the base of the toxin-fold fingers of the receptor (Fig. 2 and supplemental Table S1). Although Arg^{94} and Tyr^{91} of TGF-β1 form hydrophobic contacts with Ile^{50}, Ile^{53}, and Phe^{30} of TβRII, the majority of the interactions at this interface are either salt bridges or hydrogen bonds (Fig. 2 and supplemental Table S1). In particular, Arg^{25} and Arg^{94} of TGF-β1 form salt bridges with Glu^{119} and Asp^{32} of TβRII, respectively, that are also conserved in TβRII·TGF-β3 binary and TβRI·TBRII·TGF-β3 ternary complexes (Fig. 3*C*).

A major structural difference between the TGF-β and BMP receptor complexes is the association with their respective type II receptors. TβRII and ActRII not only bind to different sites on their ligands, Site IIa and IIb, respectively, they also use distinct residues for their ligand recognition (Figs. 4 and 5*B*). TβRII contacts TGF-β via residues from β1- and β2-strands. The secondary structure conformation of this receptor region is stabilized by a disulfide bond between Cys^{38} and Cys^{44} that is

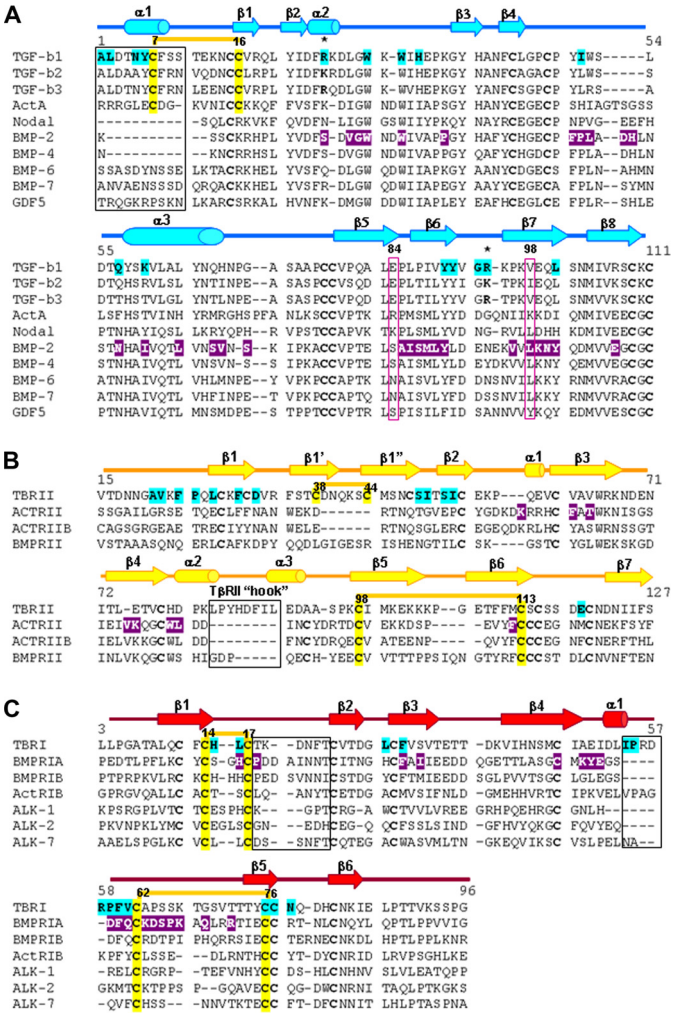

FIGURE 4. **Structure guided sequence alignment of several ligands and receptors of TGF-β superfamily.** *A*, sequence comparison of several mammalian TGF-βs, BMPs, activin, nodal and growth differentiation factor 5 (*GDF5*). The numbering is consistent with the sequence of TGF-β1. *B*, sequence comparison of several type II receptors. The numbering is according to the TβRII sequence. *C*, sequence alignment of several type I receptors. The numbering is consistent with the TβRI sequence. The secondary structure elements are illustrated as *arrows* and *cylinders* for β-strands and α-helices, respectively. The residues involved in interactions in the TGF-β1 and BMP-2 ternary complexes are highlighted *cyan* and *magenta*, respectively. Disulfide bonds critical for receptor/ligand specificity and compatibility and highlighted *yellow*, numbered, and connected by *thick yellow lines*. Secondary structure elements crucial for receptor/ligand pairing are *boxed*. Arg^{25} and Arg^{95} are marked by *stars*.

unique to TβRII. The corresponding region in all other type II receptors, including BMPRII and ActRII, lacks both β1′, β1″-strands and the Cys^{38}–Cys^{44} disulfide bond. It would result in a conformation that would sterically clash with their cytokines at Site IIa (Fig. 5, *C* and *E*). Therefore, we can conclude that Site IIa at the "tip of cytokine fingers" is unique and restricted only to TGF-β complex assembly. On the other hand, BMPs use their "knuckle site" of their fingers, Site IIb, to bind the β4 and β5 strands of their receptors. This region in TβRII contains a unique 5–8-amino acid insertion forming a hook blocking its β4 and β5 strands from binding to Site IIb (Figs. 4*B* and 5*D*). Except TβRII, other known type II receptors have significantly shorter β4-β5 loops that adopt similar conformation (Fig. 4*B*), suggesting knuckle site on cytokine is a common type II receptor binding site in TGF-β superfamily. Moreover, the β4-β5 region on type II receptors is responsible for their specificity. Here, as in the above mentioned type I receptor recognition, the shorter β4-β5 loop is characteristic for promiscuous type II receptors, such as ActRII and ActRIIB, whereas the β4-β5 loop in BMPRII, which is 3 residues longer, restricts its recognition to BMPs only.

The interface between TβRI and TβRII is the smallest of the three and is conserved in the TGF-β3 ternary complex (Fig. 3*D*). It contains predominantly hydrophobic contacts between Leu^{29}, Arg^{58}, Pro^{59}, Cys^{76}, Cys^{77}, Asn^{78}, and Gln^{79} of TβRI and Ala^{21}, Val^{22}, Phe^{24}, Pro^{25}, Leu^{27}, and Ile^{53} of TβRII (Fig. 2 and supplemental Table S1).

The type I and II receptors in TGF-β superfamily share a common three-finger toxin fold, yet have distinct binding sites, and do not appear to cross-react. Site I binding involves the residues on the first β1-β2 loop of both TβRI and BMPR-Ia. This loop is not only 7–13 residues shorter in all type I receptors (Fig. 4) but is restrained by a conserved Cys^{14}–Cys^{17} disulfide bond unique to type I receptors. Likewise, Site IIb binding is supported by a conserved disulfide bond (Cys^{72}–Cys^{84}, ActRIIA numbering) between the β5 and β6 strands present in all type II receptors but absent in type I receptors (Figs. 4 and 5*F*). The corresponding region in type I receptors assumes a different conformation stabilized by a conserved disulfide bond (Cys^{62}–Cys^{76}; Fig. 4*C*) present only in the type I receptors. Thus, the ligand recognition by the type I and II receptors of TGF-β superfamily appears to rely primarily on structural compatibilities, such as insertions and deletions at their receptor-ligand interfaces and unique disulfide bonds stabilizing specific secondary structure conformations. In general, insertions at the interface restrict the recognition, whereas deletions generate promiscuity.

TGF-β1, -β2, and -β3 Exhibit Distinct Receptor Preferences but Comparable Ternary Assembly Affinities—Despite high sequence and structure similarity among TGF-β isoforms (Fig. 4), they often cause distinct outcomes in embryonic and adult tissues (17, 19, 21, 30). These differences in TGF-βs actions might be caused by their distinct interactions with their receptors. TGF-β1 and -β3 have previously been shown to bind and assemble TβRI and TβRII into complexes in an ordered manner, first by forming a stable binary complex with TβRII and then by recruiting TβRI (31, 32). Current structures of the ternary complexes support this interdependent manner of assembly (7). To examine the receptor binding properties of the TGF-βs, we used surface plasmon resonance with TGF-βs immobilized on the sensor surface between 50 and 300 RU. The initial measurements were aimed at defining the relative affinities of TβRI and TβRII for the three isoforms. The sensorgrams obtained upon injection of TβRII over the TGF-β1, -β2, and -β3 surfaces were characterized by relatively fast on and off rates and could be readily fit using a simple 1:1 binding model (Fig. 6*A*). The derived K_D values were consistent with expectations, with both TGF-β1 and -β3 (K_D values of 190 and 140 nM, respectively) having an affinity more than a 100-fold greater than TGF-β2 (22.4 μM) (Table 2). Structurally, the TβRII interface residues Arg^{25} and Arg^{94} of TGF-β1 and -β3 are replaced with lysines in TGF-β2 (Fig. 4). This likely weakens TGF-β2 binding to TβRII because of a shorter lysine side chain and

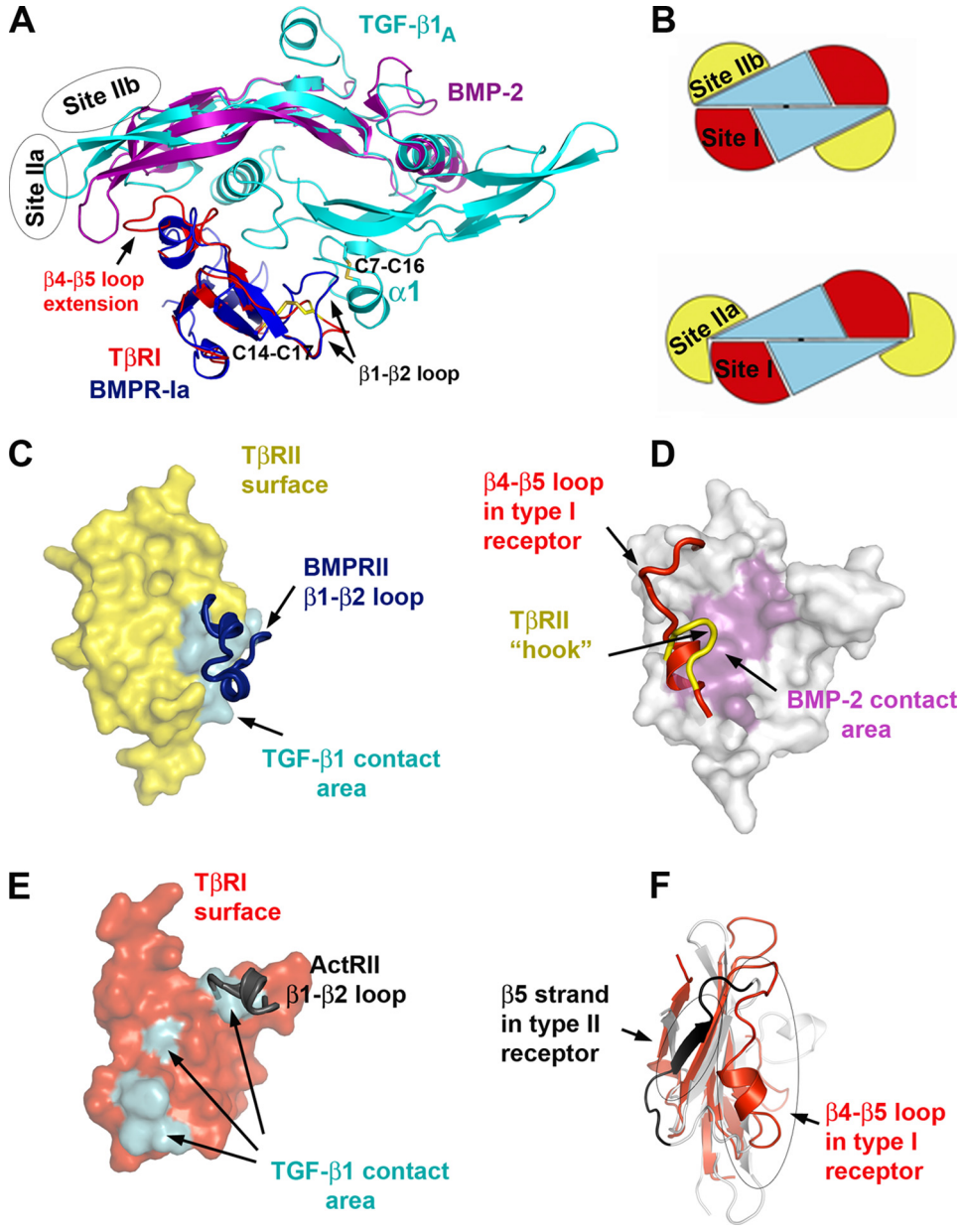

FIGURE 5. **Structural determinants critical for receptor/ligand recognition in TGF-β superfamily.** *A*, alignment of TGF-β1 and BMP-2 and their type I receptors. TGF-β1 is colored *cyan*. For clarity only one monomer of BMP-2 is shown in *magenta*. TβRI and BMPR-Ia are in *red* and *blue*, respectively. β1-β2 and β4-β5 loops as well as disulfide bonds on receptor and ligand that are critical for receptor/ligand compatibility are marked. Receptor II binding sites in TGF-β1 and BMP-2 ternary complex (Site IIa and Site IIb) are outlined as *ovals*. *B*, schematic representation of TGF-β-type and BMP-type ternary complex with receptor I and II binding sites marked as Site I, Site IIa, and Site IIb. *C*, TβRII in surface representation (*yellow*) with TGF-β1 binding site painted *cyan*. BMPRII β1-β2 loop is represented as a *blue ribbon* that blocks the binding site, thus prohibiting BMPRII from binding to Site IIa. *D*, ActRII in surface representation (*gray*) with BMP-2 contact area colored *magenta*. TβRII unique extension of β4-β5 loop (*yellow ribbon*) and unique conformation of β4-β5 loop in type I receptors (*red ribbon*) prevent binding of type I receptors and TβRII to Site IIb. *E*, surface representation of TβRI (*red*) with TGF-β1 contact area marked *cyan*. ActRII β1-β2 loop is shown as a *gray ribbon* that blocks one of the binding sites illustrating impossibility of any type II receptor to bind to Site I. *F*, critical differences in the conformation between type I (*red*) and type II (*gray*) receptors.

reduced hydrogen bond interactions (Fig. 2). Indeed, earlier substitution of Lys^{25}, Ile^{92}, and Lys^{94} with the corresponding residues in TGF-β1 and -β3 (Arg^{25}, Val^{92}, and Arg^{94}) restores high affinity TβRII binding and its ability to bind and recruit TβRI (31, 33, 34).

TβRI, to our surprise, yielded detectable signals when injected over the TGF-β2 and -β3 but not TGF-β1 surfaces (Fig. 6*B*). The TGF-β2 sensorgrams could be readily fit to a simple 1:1 binding model with a K_D of 11.2 μM, whereas the TGF-β3 sensorgrams could not. The steady state fitting of TGF-β3 sensorgrams yielded a K_D of 2.4 μM (Table 2 and supplemental Fig. S2). Interestingly, TGF-β2 binds TβRI with 2-fold higher affinity than TβRII. To attempt to quantify the weak interaction between TβRI and TGF-β1, an equilibrium experiment was performed with a higher density TGF-β1 surface (686 RU). However, the response was barely detectable over the range of TβRI concentrations sampled (0–16 μM). An estimate based on equilibrium response indicates a K_D greater than 70 μM (35). In addition to the type I receptor affinity differences between TGF-β1 and -β3, the kinetic association and disassociation rates for TGF-β3 are also slower (Fig. 6). This could contribute to the functional difference between the TGF-β isoforms. Thus, TβRI also displays ligand preferences with TGF-β3 > TGF-β2 ≫ TGF-β1. Although TβRI binds TGF-β3 tighter than TGF-β1, the interface between TβRI and TGF-β3 is 400 $Å^2$ smaller than that between TβRI and TGF-β1 because of a 10° difference in TβRI docking orientation. The structure shows that 8 of 13 TGF-β residues are conserved at the TβRI interface among the three isoforms. Asn^5, Ile^{51}, Gln^{57}, Lys^{60}, and Gln^{67} vary with Ile^{51} and Gln^{67} unique to TGF-β1 and thus may contribute to its weaker TβRI binding (Figs. 2*D* and 4*A*). Despite the fact that TβRI forms a larger interface area than TβRII with TGF-β1 and -β3, it binds both TGF-βs weaker compared with TβRII. Structurally, TGF-β1 interacts with its type II receptor mostly through hydrogen bonds and salt bridges but with its type I receptor via primarily hydrophobic contacts (Fig. 4 and supplemental Table S1). A smaller interface yet higher affinity interaction between TβRII and TGF-β1 suggests the importance of hydrogen bonds in achieving high receptor-ligand affinity. Similarly, BMP-2 forms 16 hydrogen bonds and salt bridges with its high affinity receptor BMPR-IA but mostly hydrophobic

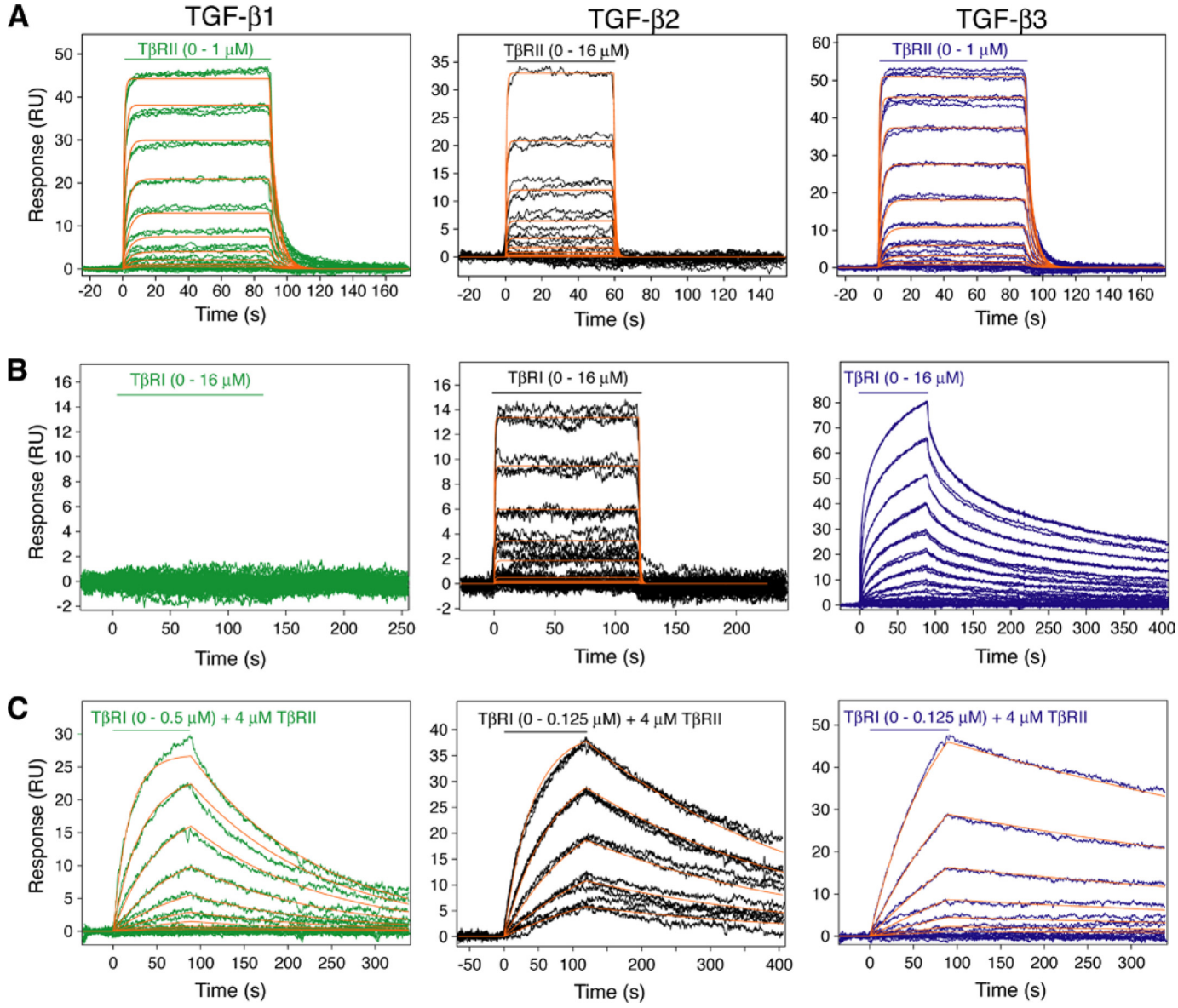

FIGURE 6. **Surface plasmon resonance sensorgrams and kinetic fits for binding of the TβRI and TβRII extracellular domains to TGF-β1, -β2, and -β3.** *A*, sensorgrams obtained as TβRII was injected. The *traces* correspond to triplicate measurements of 2-fold serial dilutions of the receptor over the concentration ranges shown. The surface densities were 185, 339, and 165 RU for TGF-β1, -β2, and -β3, respectively. The *red curves* correspond to global fits of each data set to a 1:1 binding model using Scrubber 2 software. *B*, sensorgrams and kinetic fits obtained as TβRI was injected. Surface densities were 242, 339, and 595 RU for TGF-β1, -β2, and -β3, respectively. Sensorgrams obtained for TGF-β3 indicated heterogeneity that could not be fit to a simple 1:1 model, and hence no fit is shown. *C*, sensorgrams and kinetic fits obtained as TβRI was injected in the presence of 4 μM TβRII. The surface densities were 498, 339, and 595 RU for TGF-β1, -β2, and -β3, respectively.

contacts with the low affinity ActRII. Because hydrogen bonds, in general, provide more specific receptor/ligand recognition than hydrophobic interactions, the dominance of hydrogen bonding interactions at the TGF-β1/TβRII and BMP-2/BMPR-IA interfaces is consistent with their higher affinity and thus the preferential recognition of type II receptor for TGF-βs and type I receptor for BMPs. Hydrogen bonds and salt bridges also dominate the high affinity receptor α chain binding to hematopoietic cytokines, such as interleukin-2 and -4, and van der Waal's contacts primarily occupy low affinity receptor-cytokine interfaces (36–38).

The subsequent binding studies were aimed at quantifying the extent to which one receptor type potentiated the binding of the other. To accomplish this, TβRII was included in the buffer at a concentration of 4 μM, whereas TβRI was injected over a range of concentrations. The sensorgrams obtained were characterized by slow association and dissociation rates and could each be easily fit to a simple 1:1 binding model (Fig. 6*C*). The derived K_D values were 70, 16, and 14 nM for TGF-β1, -β2, and -β3, respectively (Table 2). Thus, higher TβRI binding affinities were observed for all three TGF-β in the presence of TβRII, reflecting their similar efficiencies in assembly of the ternary complexes. Except for the case of TGF-β2 where 4 μM TβRII is 5-fold lower in concentration than their K_D, the K_D values measured for TGF-β1 and TGF-β3 reflect the binding of TβRI to the TβRII·TGF-β binary complex. Structurally, the cooperative receptor binding reflects the favorable contacts between TβRI and TβRII

TABLE 2
Dissociation and rate constants for binding of TGF-β receptors to TGF-β1, -β2, and -β3

	Analyte	Saturating receptor		TGF-β1	TGF-β2	TGF-β3
Surface plasmon resonance kinetic analysis using a 1:1 binding model	TβRI	None	K_D (μM)	ND[a]	11.2 ± 0.4	NQ[b]
			k_a (M^{-1} s^{-1})	ND	$9.6 \pm 0.3 \times 10^4$	NQ
			k_d (s^{-1})	ND	1.08 ± 0.03	NQ
	TβRII	None	K_D (μM)	0.19 ± 0.01	22.4 ± 0.5	0.14 ± 0.01
			k_a (M^{-1} s^{-1})	$1.16 \pm 0.05 \times 10^6$	$4.9 \pm 0.1 \times 10^4$	$1.8 \pm 0.1 \times 10^6$
			k_D (s^{-1})	0.22 ± 0.01	1.10 ± 0.02	0.24 ± 0.01
	TβRI	TβRII (4 μM)	K_D (μM)	0.070 ± 0.008	0.016 ± 0.002	0.014 ± 0.002
			k_a (M^{-1} s^{-1})	$9.7 \pm 0.8 \times 10^4$	$1.8 \pm 0.1 \times 10^5$	$9.6 \pm 0.3 \times 10^4$
			k_d (s^{-1})	$6.8 \pm 0.6 \times 10^{-3}$	$2.9 \pm 0.1 \times 10^{-3}$	$1.3 \pm 0.1 \times 10^{-3}$
K_D (μM) values for surface plasmon resonance equilibrium analysis	TβRI	None		>70	11.1 ± 0.4	2.4 ± 0.2
	TβRII	None		0.30 + 0.01	20.0 ± 0.8	0.17 ± 0.01
Receptor preference[c]				>200	0.5	14

[a] ND, not detectable.
[b] NQ, Not quantifiable, because sensorgrams exhibited complex kinetics and could not be adequately fit to a simple 1:1 model.
[c] Receptor preference is the ratio of the dissociation constants between the TβRI and TβRII binding separately to TGF-β. Numbers >1 indicate a preference for the type II receptor, and numbers <1 indicate that the type I receptor is preferred.

(740 $Å^2$) observed in both TGF-β1 and -β3 ternary complexes.

The close resemblance between the TGF-β1 and TGF-β3 ternary complex structures is consistent with their similar binding affinities. However, there are some important differences with regard to assembly. Although TGF-β1 and TGF-β3 both bind TβRII with high affinity, TGF-β1 binds TβRI much more weakly than TGF-β3. This difference in TβRI binding also persists in the context of the binary complexes, with the TβRII·TGF-β3 complex having a 5-fold greater affinity for binding and recruiting TβRI compared with the TβRII·TGF-β1. To better describe the receptor preference and the cooperative contribution of individual receptors in TGF-β signaling complex assembly, we define the receptor preference as the ratio of the dissociation constants between the TβRI and TβRII for each TGF-β. For example, TGF-β3 binds to TβRI and TβRII with 2.4 and 0.17 μM affinities, respectively, resulting in a 14-fold receptor preference for TβRII. This TβRII preference is estimated to be greater than 200 for TGF-β1 and vanished completely (*i.e.* 0.5) for TGF-β2. In other words, there is no preferential binding to the type II *versus* type I receptor in TGF-β2 receptor recruitment. These results demonstrate that although all three TGF-βs can effectively assemble their ternary complexes, their receptor preferences and the contribution of each receptor to the cooperative assembly appear distinct. TGF-β1, because of its strong preference for binding TβRII over TβRI, assembles ternary complex in a prototypical manner, first binding TβRII with high affinity (K_D = 190 nM) and then and only then binding and recruiting TβRI (K_D = 70 nM). TGF-β3 also preferentially binds TβRII over TβRI, although with less preference compared with TGF-β1 (Table 2). Therefore, TGF-β3 also likely binds and assembles its receptors in a largely prototypical manner. In contrast, TGF-β2 displays no receptor preference, and both receptors contribute nearly equally to the assembly of its ternary complex. This suggests that TGF-β2, instead of following the sequential receptor recruitment paradigm, engages either TβRI or TβRII and then recruits the complementary receptor or requires additional co-receptors to stabilize the binary cytokine-receptor complex. It is also possible that TβRI and TβRII associate into a preformed dimer, although no direct binding can be detected in solution between the two receptors. These results could explain the 100–1000-fold lower potency of TGF-β2 in inducing functional responses in cells lacking the TGF-β co-receptor betaglycan, because the fraction of ligand initially captured on the surface would expected to be lower for TGF-β2 compared with TGF-β1 and TGF-β3 (primarily because of its lower affinity for TβRII). Based on this, betaglycan likely functions as enhancer of cellular sensitivity to TGF-β2 by its demonstrated ability to promote binding of TGF-β2 to TβRII (39); this in turn should endow TGF-β2 with the capacity to bind and recruit TβRI in a manner comparable with that of TGF-β1 and -β3.

In summary, the structure of TGF-β1·TβRI·TβRII ternary complex and its comparison with the TGF-β3 ternary complex showed a common ligand recognition mode in the TGF-β family of cytokines by their receptors. In particular, the low affinity type I receptor interacts with both TGF-β and TβRII but with slightly different orientations at site I in the two structures. Among the type I receptors, their ligand specificity appears to correlate with the lengths of their β1-β2 ligand binding loops, with receptors with shorter β1-β2 loop being more promiscuous. The high affinity TβRII binds to a conserved site (IIa) at the tip of TGF-β1 and TGF-β3. The TβRII binding site at the tips of the cytokine fingers is restricted to TGF-β only. All other type II receptors in TGF-β superfamily bind to the common site IIb at the knuckles of cytokine. As with type I receptors, the length of the β4-β5 region is a determining factor for type II receptor specificity and promiscuity, whereby the receptors with shorter β4-β5 loop display promiscuous ligand recognition. Hydrogen bonds and salt bridges rather than hydrophobic interactions appear to be critical for the high affinity receptor recognition, in this case TβRII and TGF-β1. Unlike TGF-β1, both TGF-β2 and TGF-β3 exhibited significant affinities to TβRI. Although all three TGF-βs form their ternary receptor complexes equally well, the variations in the type I and II receptor preferences among the TGF-βs likely modulate the kinetics of ternary complex assembly. As a result, TGF-β2 likely recruits the type I and II receptors simultaneously rather than sequentially. The differences in the kinetic assembly of the type I and II TGF-β receptors suggest a potential functional variation among TGF-βs with respect to cellular and tissue distributions of their receptors.

Acknowledgments—We thank Drs. Gordon M. Joyce, Marina Zhuravleva, and the staff of the Southeast Regional Collaborative Access Team 22-ID Beamline at the Advanced Photon Source, Argonne National Laboratory for assistance in x-ray data collection. We also thank Jay Groppe for suggesting that N- and C-terminally truncated TβRI be used for crystallization and for providing the coordinates of the TGF-β3·TβRI·TβRII complex prior to publication.

REFERENCES

1. Massagué, J., Blain, S. W., and Lo, R. S. (2000) *Cell* **103,** 295–309
2. Itoh, S., and ten Dijke, P. (2007) *Curr. Opin. Cell Biol.* **19,** 176–184
3. Derynck, R., and Zhang, Y. E. (2003) *Nature* **425,** 577–584
4. Massagué, J. (1998) *Annu. Rev. Biochem.* **67,** 753–791
5. Allendorph, G. P., Vale, W. W., and Choe, S. (2006) *Proc. Natl. Acad. Sci. U.S.A.* **103,** 7643–7648
6. Greenwald, J., Groppe, J., Gray, P., Wiater, E., Kwiatkowski, W., Vale, W., and Choe, S. (2003) *Mol. Cell* **11,** 605–617
7. Groppe, J., Hinck, C. S., Samavarchi-Tehrani, P., Zubieta, C., Schuermann, J. P., Taylor, A. B., Schwarz, P. M., Wrana, J. L., and Hinck, A. P. (2008) *Mol. Cell* **29,** 157–168
8. Weber, D., Kotzsch, A., Nickel, J., Harth, S., Seher, A., Mueller, U., Sebald, W., and Mueller, T. D. (2007) *BMC Struct. Biol.* **7,** 6
9. Kirsch, T., Sebald, W., and Dreyer, M. K. (2000) *Nat. Struct. Biol.* **7,** 492–496
10. Moustakas, A., Souchelnytskyi, S., and Heldin, C. H. (2001) *J. Cell Sci.* **114,** 4359–4369
11. Itoh, S., Itoh, F., Goumans, M. J., and Ten Dijke, P. (2000) *Eur. J. Biochem.* **267,** 6954–6967
12. Derynck, R., and Feng, X. H. (1997) *Biochim. Biophys. Acta* **1333,** F105–F150
13. Daopin, S., Piez, K. A., Ogawa, Y., and Davies, D. R. (1992) *Science* **257,** 369–373
14. Hinck, A. P., Archer, S. J., Qian, S. W., Roberts, A. B., Sporn, M. B., Weatherbee, J. A., Tsang, M. L., Lucas, R., Zhang, B. L., Wenker, J., and Torchia, D. A. (1996) *Biochemistry* **35,** 8517–8534
15. Mittl, P. R., Priestle, J. P., Cox, D. A., McMaster, G., Cerletti, N., and Grütter, M. G. (1996) *Protein Sci.* **5,** 1261–1271
16. Schlunegger, M. P., and Grütter, M. G. (1992) *Nature* **358,** 430–434
17. Shull, M. M., Ormsby, I., Kier, A. B., Pawlowski, S., Diebold, R. J., Yin, M., Allen, R., Sidman, C., Proetzel, G., Calvin, D., *et al.* (1992) *Nature* **359,** 693–699
18. Kulkarni, A. B., Huh, C. G., Becker, D., Geiser, A., Lyght, M., Flanders, K. C., Roberts, A. B., Sporn, M. B., Ward, J. M., and Karlsson, S. (1993) *Proc. Natl. Acad. Sci. U.S.A.* **90,** 770–774
19. Sanford, L. P., Ormsby, I., Gittenberger-de Groot, A. C., Sariola, H., Friedman, R., Boivin, G. P., Cardell, E. L., and Doetschman, T. (1997) *Development* **124,** 2659–2670
20. Laverty, H. G., Wakefield, L. M., Occleston, N. L., O'Kane, S., and Ferguson, M. W. (2009) *Cytokine Growth Factor Rev.* **20,** 305–317
21. Kaartinen, V., Voncken, J. W., Shuler, C., Warburton, D., Bu, D., Heisterkamp, N., and Groffen, J. (1995) *Nat. Genet.* **11,** 415–421
22. Taya, Y., O'Kane, S., and Ferguson, M. W. (1999) *Development* **126,** 3869–3879
23. Shah, M., Foreman, D. M., and Ferguson, M. W. (1995) *J. Cell Sci.* **108,** 985–1002
24. Snyder, G. A., Brooks, A. G., and Sun, P. D. (1999) *Proc. Natl. Acad. Sci. U.S.A.* **96,** 3864–3869
25. Feng, X. H., and Derynck, R. (2005) *Annu. Rev. Cell Dev. Biol.* **21,** 659–693
26. Brown, M. A., Zhao, Q., Baker, K. A., Naik, C., Chen, C., Pukac, L., Singh, M., Tsareva, T., Parice, Y., Mahoney, A., Roschke, V., Sanyal, I., and Choe, S. (2005) *J. Biol. Chem.* **280,** 25111–25118
27. Allendorph, G. P., Isaacs, M. J., Kawakami, Y., IzpisuaBelmonte, J. C., and Choe, S. (2007) *Biochemistry* **46,** 12238–12247
28. Nickel, J., Kotzsch, A., Sebald, W., and Mueller, T. D. (2005) *J. Mol. Biol.* **349,** 933–947
29. Harrington, A. E., Morris-Triggs, S. A., Ruotolo, B. T., Robinson, C. V., Ohnuma, S., and Hyvönen, M. (2006) *EMBO J.* **25,** 1035–1045
30. O'Kane, S., and Ferguson, M. W. (1997) *Int. J. Biochem. Cell Biol.* **29,** 63–78
31. Zúñiga, J. E., Groppe, J. C., Cui, Y., Hinck, C. S., Contreras-Shannon, V., Pakhomova, O. N., Yang, J., Tang, Y., Mendoza, V., López-Casillas, F., Sun, L., and Hinck, A. P. (2005) *J. Mol. Biol.* **354,** 1052–1068
32. Wrana, J. L., Attisano, L., Cárcamo, J., Zentella, A., Doody, J., Laiho, M., Wang, X. F., and Massagué, J. (1992) *Cell* **71,** 1003–1014
33. De Crescenzo, G., Hinck, C. S., Shu, Z., Zúñiga, J., Yang, J., Tang, Y., Baardsnes, J., Mendoza, V., Sun, L., López-Casillas, F., O'Connor-McCourt, M., and Hinck, A. P. (2006) *J. Mol. Biol.* **355,** 47–62
34. Baardsnes, J., Hinck, C. S., Hinck, A. P., and O'Connor-McCourt, M. D. (2009) *Biochemistry* **48,** 2146–2155
35. Radaev, S., and Sun, P. D. (2001) *J. Biol. Chem.* **276,** 16478–16483
36. Wang, X., Lupardus, P., Laporte, S. L., and Garcia, K. C. (2009) *Annu. Rev. Immunol.* **27,** 29–60
37. Rickert, M., Boulanger, M. J., Goriatcheva, N., and Garcia, K. C. (2004) *J. Mol. Biol.* **339,** 1115–1128
38. LaPorte, S. L., Juo, Z. S., Vaclavikova, J., Colf, L. A., Qi, X., Heller, N. M., Keegan, A. D., and Garcia, K. C. (2008) *Cell* **132,** 259–272
39. López-Casillas, F., Wrana, J. L., and Massagué, J. (1993) *Cell* **73,** 1435–1444
40. Zou, Z., and Sun, P. D. (2004) *Protein Expr. Purif.* **37,** 265–272
41. Cerletti, A., Drewe, J., Fricker, G., Eberle, A. N., and Huwyler, J. (2000) *J. Drug Target* **8,** 435–446
42. Hinck, A. P., Walker, K. P., 3rd, Martin, N. R., Deep, S., Hinck, C. S., and Freedberg, D. I. (2000) *J. Biomol. NMR* **18,** 369–370
43. Otwinowski, Z., and Minor, W. (1997) *Methods Enzymol.* **276,** 307–326
44. McCoy, A. J., Grosse-Kunstleve, R. W., Adams, P. D., Winn, M. D., Storoni, L. C., and Read, R. J. (2007) *J. Appl. Crystallogr.* **40,** 658–674
45. Kissinger, C. R., Gehlhaar, D. K., and Fogel, D. B. (1999) *Acta Crystallogr. D Biol. Crystallogr.* **55,** 484–491
46. Kleywegt, G. J., and Jones, T. A. (1997) *Methods Enzymol.* **277,** 208–230
47. Emsley, P., and Cowtan, K. (2004) *Acta Crystallogr. D Biol. Crystallogr.* **60,** 2126–2132
48. Brünger, A. T., Adams, P. D., Clore, G. M., DeLano, W. L., Gros, P., Grosse-Kunstleve, R. W., Jiang, J. S., Kuszewski, J., Nilges, M., Pannu, N. S., Read, R. J., Rice, L. M., Simonson, T., and Warren, G. L. (1998) *Acta Crystallogr. D Biol. Crystallogr.* **54,** 905–921
49. Adams, P. D., Grosse-Kunstleve, R. W., Hung, L. W., Ioerger, T. R., McCoy, A. J., Moriarty, N. W., Read, R. J., Sacchettini, J. C., Sauter, N. K., and Terwilliger, T. C. (2002) *Acta Crystallogr. D Biol. Crystallogr.* **58,** 1948–1954
50. Collaborative Computational Project, Number 4 (1994) *Acta Crystallogr. D Biol. Crystallogr.* **50,** 760–763